Physics and Imaging in Radiation Oncology 22 (2022) 123–130

Contents lists available at ScienceDirect

Physics and Imaging in Radiation Oncology

journal homepage: www.sciencedirect.com/journal/physics-and-imaging-in-radiation-oncology

Monte Carlo calculations of radiotherapy dose distributions within and around orthopaedic implants

Georgio Andrew Katsifis *, David R. McKenzie, Natalka Suchowerska

VectorLAB-School of Physics, University of Sydney, Sydney, Australia

ARTICLE INFO

Keywords:
Monte Carlo
Orthopaedic implants
Regenerative medicine
3D Printing
PEEK
Titanium
Radiation dosimetry

ABSTRACT

Background and purpose: Cancer patients often require a titanium orthopaedic implant to support or replace lost bone. In radiation treatment, the dose distribution is perturbed causing regions of high and low dose at material interfaces. Since the survival of integrating bone tissue is critical to implant success, the aim of this study was to determine the dose distribution in and around the scaffold, when constructed from titanium or Poly-ether-ether-ketone (PEEK).

Materials and methods: The dose distributions in the pores and along boundaries for three implant scaffold designs were calculated using Monte-Carlo methods in Geant4/GATE, with the material taken as titanium or PEEK. The 3D dose distributions were analysed in MATLAB and segmented using image masks, yielding the dose distributions in key regions of interest. To evaluate the effect of the predicted dose perturbations, the cell survival was calculated using the linear-quadratic model for SAOS-2 cells (bone) using experimentally determined radiation response data.

Results: High dose gradients were found along the boundaries of the titanium implants, but not for the corresponding PEEK implants. The dose to the internal cavities of the titanium implants was enhanced by 10–15% near the proximal interface whereas for PEEK, there was no significant dose perturbation. The predicted perturbation caused by the titanium implant was shown to decrease the survival for SAOS-2 cells by 7% which was not found for the PEEK implants.

Conclusion: PEEK was shown to be a more favourable orthopaedic implant material over titanium for cancer patients considering radiation therapy.

1. Introduction

Cancer patients frequently present for radiotherapy with titanium implants, with head and neck cases being particularly challenging to plan. The patient computer tomography (CT) and cone beam computer tomography (CBCT) images were created using kV x-rays which show image artefacts and may obscure critical information at the bone-implant interface. The patient treatment dose is perturbed by the titanium, creating low and high dose regions, which are known to be poorly predicted by treatment planning systems [1,2]. The practical implication of a high dose region in the vicinity of the implant could compromise healing and regeneration of bone, with the ultimate risk of infection and implant failure, requiring major surgical revision, especially in the case of the spinal cord should re-irradiation be required. Conversely, any cancer cells in a low dose region will be under-treated, potentially leading to a recurrence [3,4].

Bone prosthetic implants have typically been constructed as solid metal objects. In an attempt to reduce the effective stiffness of the implant, reduce stress shielding and to allow for increased osseointegration, customised 3D printed porous structures have become available [5,6]. Conversely, in a radiation field, it is not immediately obvious how the titanium scaffold might perturb the dose inside the scaffold, affecting the regenerating tissue inside the pores, which will in turn affect the success of the implant.

For simple beam arrangements and implant designs, the dose distribution has been reported. Nevelsky, Akyol and Müller provided evidence for significant dose enhancements (~20%) on the entrance interface of a titanium object and a large dose reduction (~20%) on the exit interface [1,2,7]. For a cylindrical meshed metallic stent, with a lower effective density than the shell stent of identical volume, Li et al., found that the lower effective density reduced the expected perturbation of both a 6MV and a 15MV photon beam [8], indicating that the porosity

* Corresponding author.
E-mail address: gkat2146@uni.sydney.edu.au (G.A. Katsifis).

https://doi.org/10.1016/j.phro.2022.04.011
Received 29 September 2021; Received in revised form 26 April 2022; Accepted 27 April 2022

of the metal object is a significant factor affecting the dose distribution. While studies using Monte Carlo (MC) simulation and experimental measurement have determined the dose perturbation caused by metal structures [9], they have not reported on the dose within the pores of a bone implant scaffold and along the interfaces of the material.

MC simulation is ideally suited to this task, because of the difficulty in taking measurements with sufficient spatial resolution within the fine pores of a scaffold implant. While film dosimetry provides high spatial resolution, the porous implant designs typically have complex geometries with pore diameters in the order of 0.5 mm or less, which makes it difficult if not impossible to position the film. However, film dosimetry has been successfully used to measure the dose distribution at the implant tissue interface [2,9]. MC also gives the option to understand the fundamental physics explaining the dose distribution by differentiating between particles of different origins and trajectories.

Here a simulation study was presented for three implant designs. The traditional titanium and an emerging implant material, poly-ether-ether-ketone, (PEEK) were used as implant materials. Thermoplastics of the poly-aryl-ether-ketone (PAEK) family, including PEEK, are emerging as an alternative, because they provide a better material property match to bone and are reported to cause minimal dose perturbation [10]. Due to their lower effective atomic number and density, these carbon based plastics exhibit almost tissue-equivalent radiation scattering properties between the 10 keV and 10 MeV range of energies (with $Z_{eff} = 6.26$ and $\rho = 1.32 g/cm^3$ and reduced dose perturbation relative to titanium [11,12]. A reference to the attenuation coefficients as a function of photon energy are shown in the Supplementary material A (Figure A). PEEK is of particular interest, as it is biocompatible, has a higher elastic modulus than most polymers (3–4 GPa), lying between the modulus for cancellous (1 GPa) and trabecular (14 GPa) bone [13–18]. PEEK can also be 3D printed, enabling implants to be quickly customised for individual patients and manufactured with porosity to facilitate osseointegration.

Our aim is to describe the dose distribution for these structures, two of which are currently used in head and neck orthopaedic surgery. The novelty of this study was that it enabled us to determine the dose distribution within the micro-structures of complex geometries rather than just on the external interfaces and provides insight on specific features of the implant which can reduce the perturbations to osseointegrating cells. The second aspect of this study provided a measure of risk to the osseointegrating cells in and around implants constructed from titanium and PEEK.

2. Materials and methods

2.1. Monte Carlo

The dose distribution was determined with Monte Carlo (MC) methods using the Geant4 (v10.02.p04) toolkit in Gate v8.0 [19] and validated against calibration data measured on a Varian Truebeam™ Linac. Fig. 1 shows three implant designs used; the first is a generic reconstruction plate (referred to as “rings”), the second is a simple geometric design with orthogonally assembled, parallel, filament arrangement (referred to as “woodpile”) and the third is a titanium reconstruction plate customised for an individual patient (referred to as “Mesh”). To simulate the dose distribution in these 3 periodically arranged pore structures, they were each unfolded to a flat x-y plane, shown in Fig. 1. Each implant in turn was simulated in a 30 × 30 × 30

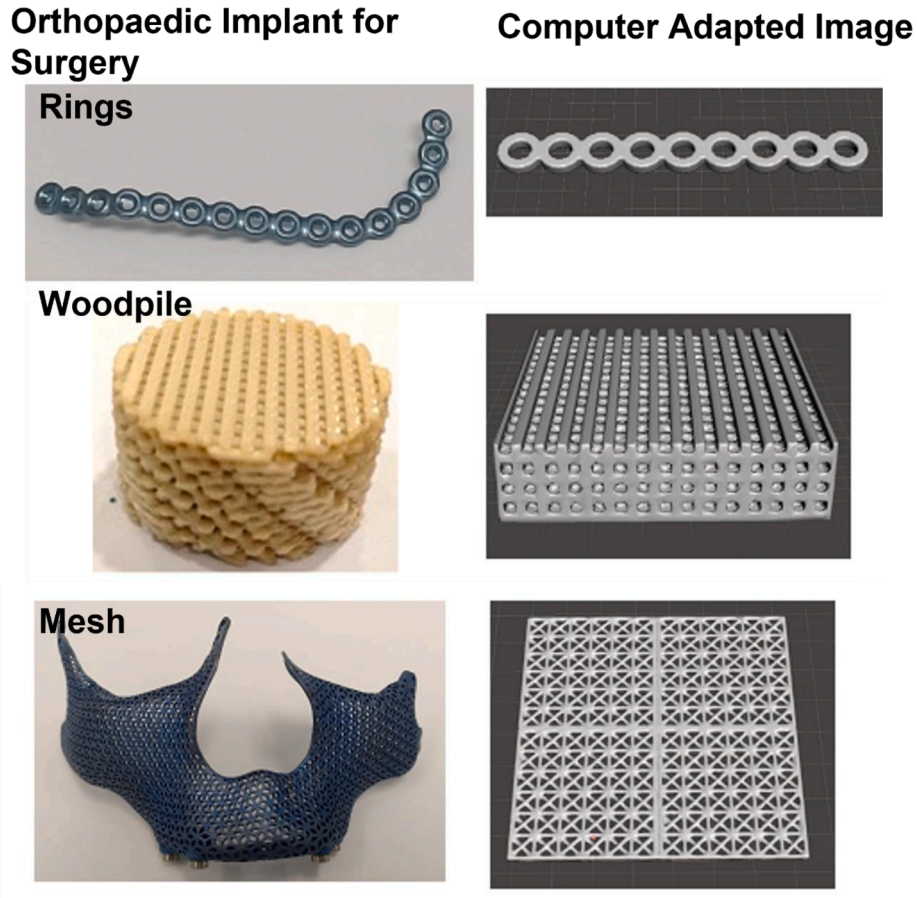

Fig. 1. The three orthopaedic implant designs used in the simulation are shown on the left, with the adapted image used to generate the simulation geometry shown on the right. The unfolded STL files are labelled from the top down: Rings; Woodpile Scaffold; Facial Mesh.

cm^3 water phantom located at a depth of 5 cm and irradiated with a 6MV photon beam with the SSD at 100 cm and a field size of 5×5 cm^2. The 6MV Varian Truebeam™ beam spectrum was obtained using the "energy spectrum actor" in GATE, from the phase space file provided [20]. A summary of the geometric beam setup, exact dimensions and scoring parameters appears in the Supplementary material B (Figure B) along with the range and energy cuts for the simulation.

The attenuation coefficients for titanium and water were taken from the National Institute for Standards and Technology (NIST) database [21]. The pores in the simulation were taken to be water as a first approximation towards regenerating bone tissue, which typically contains little mineralisation at the time of irradiation following surgery. This was confirmed in a pilot animal study using micro-CT to determine the HU and density in the pore of the scaffold.

PEEK material was defined in GATE by using the values of its constituent elemental composition as input data. Materials databases for water and titanium were supplied in GATE, while PEEK was composed of fractions of carbon, hydrogen and oxygen in accordance with its molecular structure, with the attenuation calculated using a weighted sum of attenuation coefficients. Where a_i represents the fraction of each molecule/atom for PEEK.

$$\frac{\mu}{\rho}_{total} = \sum_i a_i \left(\frac{\mu}{\rho}\right)_i \tag{1}$$

The percentage depth dose in the direction of the incident beam (z-axis) through the phantom was scored with a resolution of 0.5 mm. The dose profile, perpendicular to the beam z-axis through the implant and adjacent layers was also scored at 0.5 mm. The dose values were exported as one dimensional (.txt) files and analysed in MATLAB 2019b. The simulations were then performed across a smaller volume bounding the implant, with dosel (voxelised regions recording the dose) sizes specified in the Supplementary material B (Table B). The measurements were saved as image (.mhd) files and converted to csv files in Python 3.7.0™ and exported to MATLAB 2019b™, where the dosimetric quantities were analysed as 3 dimensional matrices. The simulation was repeated for each implant with the material being either PEEK or titanium.

2.2. Creating binary scaffold masks

The new, integrating bone cells on the external and internal surfaces of the scaffold were taken to be the regions of interest. Each mask was created to determine the dose to the volume occupied by the pores of the implant. For the "ringed" implant, the mask was created by generating circles, with a radius of 2.5 mm centred on the pores using the poly2-mask function, specifying the region of interest with 360 points. The scaffold implant was created using a binary 2-D matrix with alternating columns of 1's and 0's, effectively removing the scaffold columns from the dose distribution. The mask for the third implant structure was created using the "make pattern" function in Autodesk Meshmixer™. The STL file was imported as a patch file into MATLAB. All the vertices of the STL structure were mapped onto a plane, which traced out the cross-section of the structure. To ensure accurate, mapping of the cross-section, the mesh density of the 3D structure was increased in Meshmixer before importing. The generated masks and the corresponding dose distributions are shown in the Supplementary material C (Figure C).

2.3. Calculating the integrated dose

With the 3D dose distributions, the dose was integrated along the z and x-axes Cartesian axes to generate the percentage depth dose curves and dose profiles. The water phantom containing the implant is denoted as the region W, which contained each implant denoted as S_j, such that the implant was contained in the water phantom $S_j \subset W$. For the depth dose curves shown in supplementary D (Figure D), the dose was scored in a $10 \times 10 mm^2$ region along the central axis of the implant. To calculate the dose closer to the implants, the dose was integrated on each surface layer δS_i which contains both the implants and the pores. The dose was calculated in discrete dosels as follows:

$$D(z) = \int_{S_i}\int D(x,y,z)dxdy \approx \sum_{-a}^{+a}\sum_{-b}^{+b} D(x_i,y_j,z)\Delta x_i \Delta y_j \tag{2}$$

Where $D(x,y,z)$ is the 3D dose distribution, [-a,a] and [-b,b] map the boundaries of the implant in the x-y plane and Δx_i and Δy_i are the dosels widths. The dose profile, along the x-axis was calculated similarly as:

$$D(x) = \int_{S_i}\int D(x,y,z)dydz \approx \sum_{-b}^{+b}\sum_{-c}^{+c} D(x,y_i,z_j)\Delta y_i \Delta z_j \tag{3}$$

Where Δz_i is the voxel size and [−c,c] are the bounds of the implant in the z direction and some additional volume of water before the proximal interface and after the exit interface. The dose within the pores of the implant was calculated by multiplying the dose distribution $D(x,y,z)$, within the regions S_j by the binary masks $M_j(x,y,z)$. Here $i = 1:3$ and denotes the three masks used. Thus, the dose distribution within the pores was calculated along the z and × axes as:

$$\begin{aligned} D(z)_{pores} &= \int_{-b}^{+b}\int_{-c}^{+c} D(x,y,z)M(x,y,z)dydz \\ &\approx \sum_{-b}^{+b}\sum_{-c}^{+c} D(x_i,y_j,z)M(x_i,y_j,z)\Delta y_i \Delta z_j \end{aligned} \tag{4}$$

$$\begin{aligned} D(x)_{pores} &= \int_{-b}^{+b}\int_{-c}^{+c} D(x,y,z)M(x,y,z)dydz \\ &\approx \sum_{-b}^{+b}\sum_{-c}^{+c} D(x,y_i,z_j)M(x,y_i,z_j)\Delta y_i \Delta z_j \end{aligned} \tag{5}$$

The 2D integration was calculated using Simpson's rule in 2D [22]. Figs. 2–4 show the 2D dose profiles along the proximal interface, the central axis depth-dose curves and the dose profiles along the x axis, for a range of depths through the implant structure, for PEEK and titanium. The figures are presented in the following order: "ringed", "woodpile" and "mesh". The depth dose curves of Figs. 2-4, c and d are normalised to the dose in water at d = 5 cm. This normalisation makes it easier to visualise the dose perturbations at the entrance interface due to the titanium and PEEK implants. For the profiles in Figs. 2-4 e, the dose was normalised to the central axis at x = 0 cm for water. Figs. 2-4 d depicts the corresponding depth dose distribution within the pores of each structure. Fig. 5 summarises the absorbed dose to the pores of each implant for each material. The change in dose at three depths (entrance interface, middle of the implant and exit interface) were plotted for both PEEK and titanium, with the corresponding error bars calculated from the standard error of the dose to water. Uncertainty in the MC simulation was within 2% and specific uncertainties for each simulation is given in the Supplementary material (Table F).

2.4. Calculating cell survival

To assess the impact of the perturbed dose on the integrating cells, cell survival was calculated from the simulated dose using the linear quadratic model with α and β parameters determined from measured data for the SAOS-2 cell line, as shown in equation (6).

$$SF(D) = \exp\left(-\alpha D - \beta D^2\right) \tag{6}$$

Where D is the dose in Gy, α and β are the radiobiological parameters. The parameter values $\alpha = 0.37 Gy^{-1}$ and $\beta = 0.2 Gy^{-2}$ [23] were used and the results are plotted in Fig. 6. Survival fraction was first calculated from 0 to 3 Gy for irradiation in the absence of an implant. The SAOS-2 cancer cell line was chosen because it displays several features similar to normal osteoblasts are commonly used as anaolgues for them. The SAOS-2 cells differentiate in a similar manner and can deposit mineralisation on an extracellular matrix. We have therefore used these cells

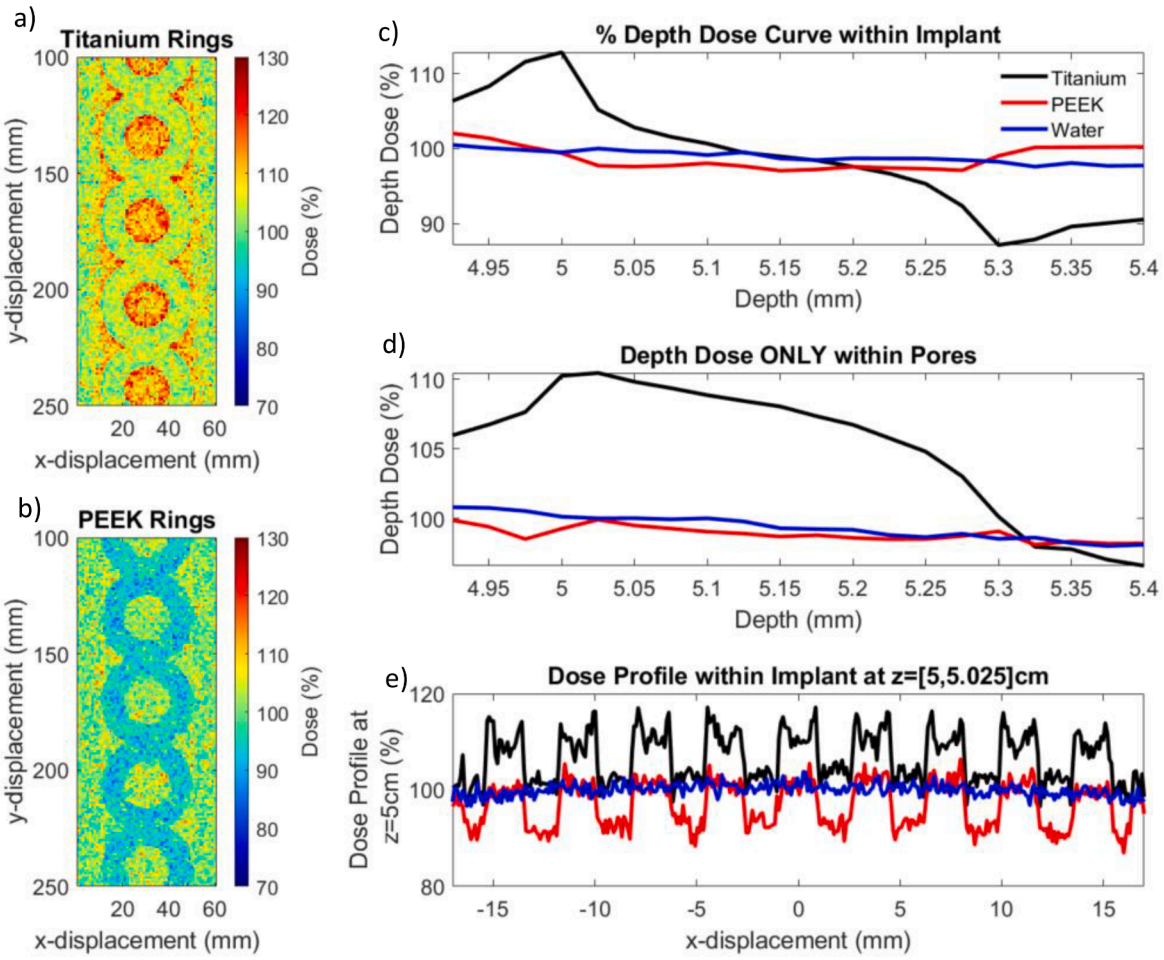

Fig. 2. 2D Dose profiles for titanium and PEEK "ringed" scaffolds (a, b), with the corresponding percentage depth dose curves (c–e). Figure (c) shows the depth dose curve normalised to water at z = 5 cm for titanium and PEEK scaffolds. Figure (d) shows a plot of the depth-dose distribution in the pores of the scaffold. Figure (e) shows the lateral profile, taken along the central y-axis of the dose profiles in figures (a,b) for the same conditions, normalised at × = 0 cm.

in our radiobiological modelling [24,25].

To obtain the survival fractions arising from the dose perturbation caused by implants, the dose was multiplied by the perturbation factors as calculated in Fig. 5. Thus, the survival fraction was calculated as a function of the primary dose administered to water.

$$SF(D) = \exp(-\alpha DP(z) - \beta(DP(z))^2) \quad (7)$$

Where $P(z)$ is the perturbation factor at different depths z for each implant. The dose-survival curves were plotted for each implant in PEEK and titanium, for the perturbation factors calculated at the proximal interfaces ($z = 5cm$).

3. Results

Fig. 2c shows that on the proximal tissue-implant interface, there was a 15% increase in dose when the implant material is titanium and <5% when it was PEEK. At the exit interface, the reduction in dose was of the order of 10% for titanium and an enhancement of 5% for the PEEK implant. In Fig. 2d, where only the dose to the pores of the implant was shown, a dose maximum was observed for the pore of the titanium ring, however, it was not a sharp gradient as seen at the entrance and exit interface, but a broader peak with a significant, albeit reduced enhancement of 12%. The maxima also occurred at a slightly deeper position within the pore, rather than at the implant tissue interface. For the PEEK pores, there was a slight reduction in dose before the proximal interface of 2%, however within the pore, the perturbations were minimal. The dose profile in Fig. 2e shows that there were sudden changes in dose depending on the relative location of the pores in the titanium/PEEK rings. For the titanium rings, there was a sharp increase in dose between 16 and 18% at the implant-pore boundary of the ring. This was generally followed by a reduction in dose to a local minimum within the pore, ranging from 8 to 12% and subsequently other maxima towards the pore to implant edge. The dose in the actual titanium implant remained close to that of water at the proximal interface. In comparison, the dose profile corresponding to the PEEK implant had a similar shape to the titanium but was shifted down by 10%. Within the pores of the PEEK rings, the dose remained within 2–5 % of the dose to water. The local minima in dose that was observed in the pore of the titanium implant were not present within the PEEK. The dose within the bulk of the PEEK implant was between 5 and 10% lower than the dose to water.

The characteristic dose enhancements and reductions from titanium are shown in Figs. 3-4 at the entrance and exit interfaces (c) and as previously shown in Fig. 2, demonstrate sharp changes in dose at most cavity-implant boundaries. Fig. 3c, shows that the dose distribution behaves somewhat like a sawtooth function and varied between sharp maxima and broad minima. For the titanium implant, the dose reached a maximum at 18% at the proximal interface, unlike for PEEK where the dose remained unperturbed compared to water. The reduction in dose compared to water shown in Fig. 3c refers to the dose within the PEEK implant and was a small reduction (<5%). Fig. 3d shows the sawtooth behaviour seen in Fig. 3c. The maximum dose occurs at the point where the layers alternate in orientation.

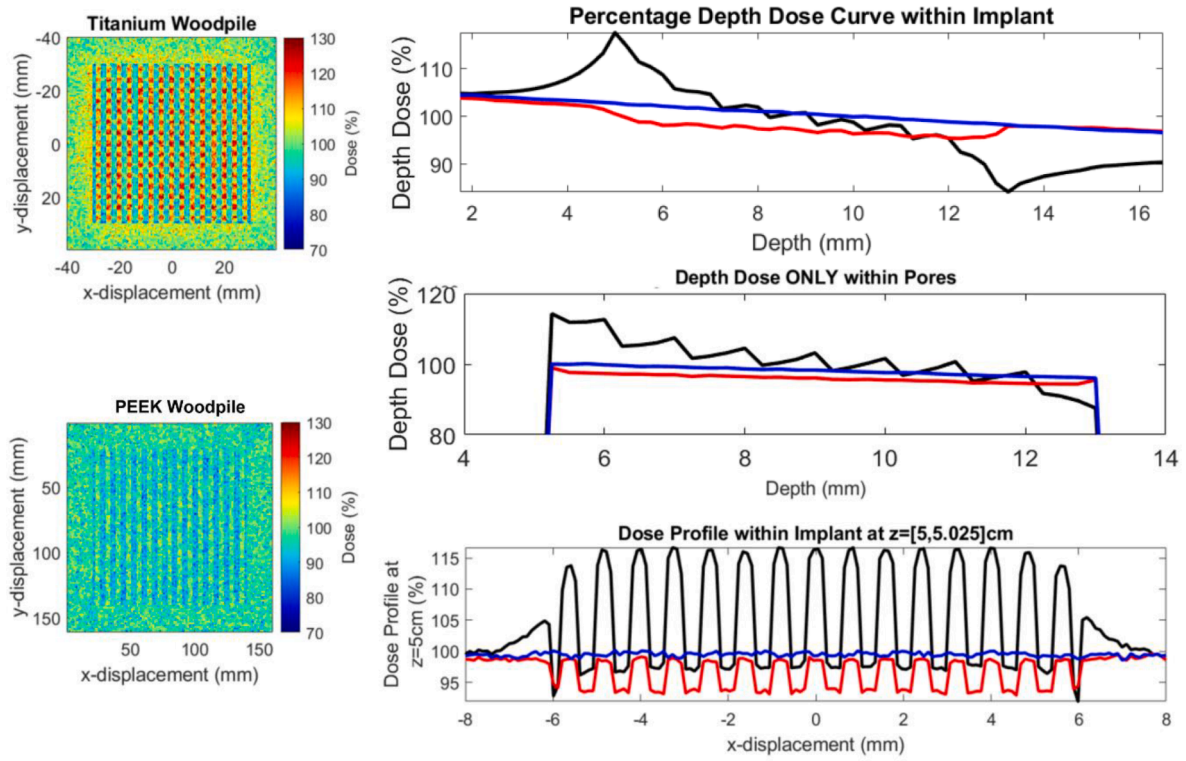

Fig. 3. 2D Dose profiles for titanium and PEEK "woodpile" scaffolds (a,b), with the corresponding percentage depth dose curves (c-e). Figure (c) shows the depth dose curve normalised to water at z = 5 cm for titanium and PEEK scaffolds. Figure (d) shows a plot of the depth-dose distribution in the pores of the scaffold. Figure (e) shows the lateral profile, taken along the central x-axis of the dose profiles in figures (a, b) for the same conditions, normalised at × = 0 cm.

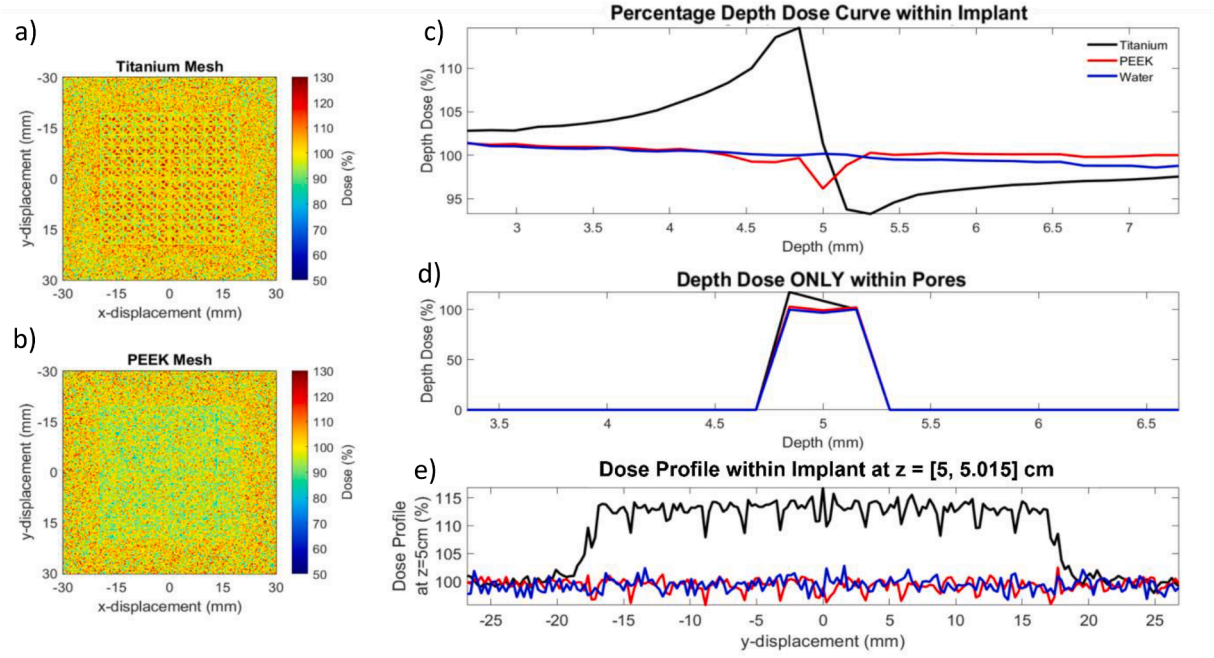

Fig. 4. 2D Dose profiles for titanium and PEEK "mesh" scaffolds (a, b), with the corresponding percentage depth dose curves (c–e). Figure (c) shows the depth dose curve normalised to water at z = 5 cm for titanium and PEEK scaffolds. Figure (d) shows a plot of the depth-dose distribution in the pores of the scaffold. Figure (e) shows the lateral profile, taken along the central x-axis of the dose profiles in figures (a,b) for the same conditions, normalised at × = 0 cm.

The perturbations of dose within the pores of the PEEK implant were small (<2%), whereas for titanium the dose distribution exhibited a sawtooth behaviour. For each set of alternating layers in titanium, the dose can increase or decrease by 2–7% and was also depth dependent. Fig. 3e depicts the dose profile for the "woodpile" structure and shows a large increase in dose within the first layer for the titanium structure of 18% and a minimum corresponding to a reduction of −7% towards the scaffold boundaries and −2% within the structure. The dose profile for PEEK shows similar behaviour with the dose maxima were observed to remain within 1% of the dose to water and the dose minima correspond

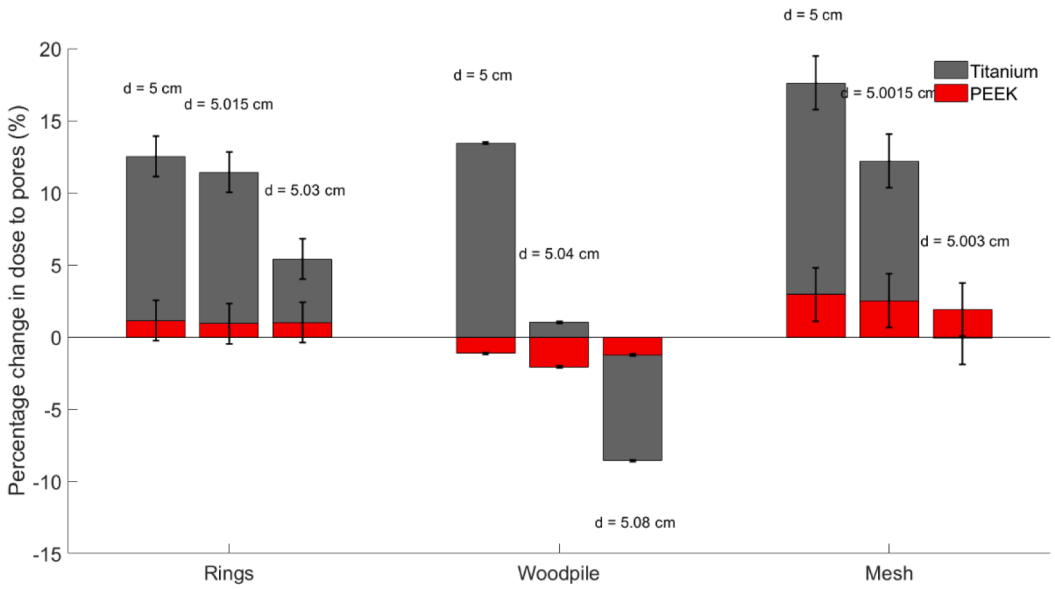

Fig. 5. The percentage change in dose to the pores of the implants with reference to water at three different distances d through the pores (at the proximal interface, halfway and at the exit interface), for PEEK (red) and titanium (grey) materials. The error bars are calculated from the standard error of the dose to water at the 100% dose reference plane. The standard error in dose is found to be higher in the smaller pores in the facial mesh implant.

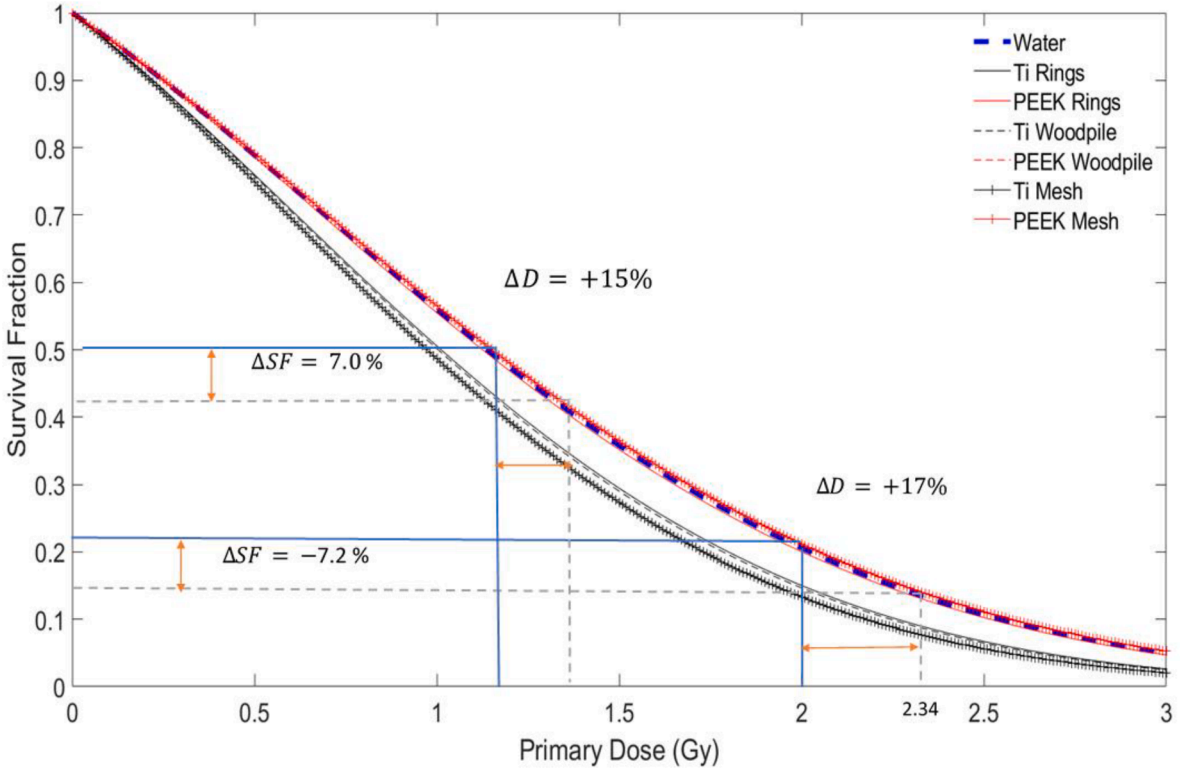

Fig. 6. Calculated survival fraction as a function of radiation dose for the osteosarcoma, SAOS-2 cell line. The survival fractions corresponding to the osteosarcoma cells within the pores of the titanium and PEEK implants are also plotted for all three designs.

to reductions of −7%.

Fig. 4 shows dose distributions for the facial mesh structure. The dose enhancement and reduction arising from the titanium were similar in magnitude to those calculated previously, with similarly shaped dose distributions, most notably for the depth dose curves in Fig. 4c and d. A significant enhancement of dose (>15%) was observed within the implants, despite the very small thickness (<0.5 mm).

4. Discussion

In this study, it was found that the geometry of the implant can significantly impact the dose distributions within the micro-structures. While these effects were more prominent for titanium, they were still present for PEEK implants. The dose profiles of Figs. 2-4e further demonstrate the sudden dose gradients which occurred in the titanium implant, located at the pore-titanium interface. Previous studies, which

have predominantly focused on the dose to the exterior interfaces as measured by Akyol, Nevelsky and Müller [1,2,7], show agreement with the results of this paper. The dose perturbations at the proximal and exit interface that arose from titanium were found to vary between 15 and 20% with discrepancies arising from geometric and irradiation factors. However, the limitation of these studies was that they only focused on the proximal and exit interfaces of the implant and used simple geometric arrangements. By concentrating on the internal geometries of the implant, the steep dose gradients arising between the interfaces of tissue and titanium were identified. The increase in dose at the titanium-tissue interface arises from an increase in secondary electrons which deposit more of their energy close to the boundary of the implant. This was especially pronounced for the ringed implant in Fig. 2, where the higher dose is present as a red region along the exterior boundary, along the inner circumference of the ring and as sharp dose gradients in the profile in Fig. 2e. When these implants were constructed from PEEK, there was still a dose gradient with the maximum dose remaining close to water. For greater visibility, the high and low dose regions within the pores of the ringed scaffold are shown in supplementary E. However, the significant dose reduction is only observed within the physical implant of PEEK and not in the tissue. These doses should be of no concern to the regenerating tissue.

For the woodpile structure, the unique feature lies in the sawtooth behaviour in the depth dose curves as shown in Fig. 3c-d, for both PEEK and titanium implants. In both instances, the sawtooth arises from the alternating forward and backwards scatter of secondaries as the primary photon beam alternates between layers. This region of increased dose was also shown in Fig. 3a where the increased dose from the back scatter can be seen as a set of horizontal lines, partially covered from the solid titanium layer above. For the woodpile implant constructed from titanium, such a microstructure possesses high dose gradients from both backscattered and laterally scattered electrons enveloping the internal surfaces resulting in high doses administered to regenerating cells. For the PEEK woodpile implant, while the sawtooth behaviour was present, the maximum doses were within a safe margin of that to water.

The dose within the meshed implant displayed similar behaviour to the other implants with the characteristic increase and decrease in dose at the proximal and exit interfaces. Within the structure of the implant, the pores were still subjected to high doses (10% increase) even with the small thickness of the implant. Given the small size of the pores, the laterally scattered secondaries from the titanium contribute greatly to the marked dose enhancement. Compared to the other implants, there is a greater degree of statistical variance due to the reduced sample size, by the application of the binary mask. The close proximity and spacing of the pores result in regions of sharp dose gradients, which are masked when computing the surface integral over the whole surface.

For all cases the radiation dose was observed to be highest in the tissue directly above the implant entrance interface for titanium and within the pores for the first half of the scaffold implant, closer to the entrance interface as shown in Fig. 2d. The regenerating bone on these surfaces are therefore at the highest risk of adverse radiation effects. In contrast, when the same scaffold was made from PEEK, the dose to the pores throughout the scaffold implant was closer to that expected in water and in the absence of an implant. Furthermore, due to the water-equivalent attenuation properties of PEEK and relatively homogenous dose distribution, imaging will not incur artifacts and commercial treatment planning is likely to be more accurate than for titanium implants [2]. For patients who require radiotherapy and implant as a result of surgery, it is critical that radiotherapy is started as soon as the bone has sufficiently healed [9].

The survival fraction for the SAOS-2 cell line, calculated using the linear quadratic model as illustrated in the method and the curves plotted in Fig. 6. For an administered dose of 2 Gy to the implant surface, the equivalent dose to the cells within a PEEK scaffold was approximately 2 Gy, however for the titanium implant, the equivalent dose was 2.34 Gy, which translates to a reduction in survival of 7.2%. Alternatively, for the weakly perturbing PEEK implant, the survival fraction is unchanged. An error of 5% in dose delivery is considered an incident in radiotherapy. For a given dose enhancement of approximately 15%, the survival is reduced by a further 7.2%, which can impact outcomes such as tumor control probability (TCP) and normal tissue toxicity. Given the inhomogenous dose distributions within the volume of the titanium implant, there will be regions where tissue toxicity is high and tumor control is low. For implants which are osseointegrating, it is important to consider the change in survival fraction in order to avoid subsequent potential implant failure, osseonecrosis and even reversal surgery [26].

These findings are important since there are claims that radiotherapy patients are overrepresented in the group of patients requiring surgical reversal of implants, although it is difficult to find conclusive data in the literature since patients requiring substantial implants are also likely to have more advanced cancers and do less well. The results presented here are evidence of increased dose to the regenerating cells about a titanium implant and within the pores of a scaffold implant design, of a magnitude likely to have a significant biological effect. Furthermore, any cancer cells populating shielded surfaces within the titanium implant are at a risk of being underdosed, potentially compromising the radiotherapy treatment. The same implant constructed from PEEK will not exhibit this dose perturbation, avoiding all the additional steps that have been incorporated into radiotherapy to correct for a titanium object in the beam.

Data availability statement for this work

All data is available upon request from the corresponding author. Email at gkat2146@uni.sydney.edu.au.

Funding statement

I would like to acknowledge the funding support from the: National Health and Medical Research Council Grant number GNT1183597.

Declaration of Competing Interest

The authors declare that they have no known competing financial interests or personal relationships that could have appeared to influence the work reported in this paper.

Acknowledgements

We acknowledge that all work was performed solely by the authors of this paper unless otherwise specified. This project was undertaken at the University of Sydney, School of Physics, Department of Applied and Plasma Physics-VectorLAB.

We acknowledge Xue Yang, for installing GATE on the cluster and helping me run the scripts efficiently. We acknowledge Brad Oborn for a productive discussion on running Monte Carlo and in setting up my simulation geometry.

Appendix A. Supplementary data

Supplementary data to this article can be found online at https://doi.org/10.1016/j.phro.2022.04.011.

References

[1] Nevelsky A, Borzov E, Daniel S, Bar-Deroma R. Perturbation effects of the carbon fiber-PEEK screws on radiotherapy dose distribution. J Appl Clin Med Phys 2017; 18:62–8. https://doi.org/10.1002/acm2.12046.

[2] Akyol O, Dirican B, Toklu T, Eren H, Olgar T. Investigating the effect of dental implant materials with different densities on radiotherapy dose distribution using Monte-Carlo simulation and pencil beam convolution algorithm. Dentomaxillofacial Radiol 2019;48:20180267. https://doi.org/10.1259/dmfr.20180267.

[3] Eaton DJ, Byrne JP, Cosgrove VP, Thomas SJ. Unintended doses in radiotherapy-over, under and outside? Br J Radiol 2018;91:20170863-. https://doi.org/10.1259/bjr.20170863.
[4] Knöös T. Lessons Learnt from Past Incidents and Accidents in Radiation Oncology. Clin Oncol 2017;29:557–61. https://doi.org/10.1016/j.clon.2017.06.008.
[5] Simon U, Augat P, Ignatius A, Claes L. Influence of the stiffness of bone defect implants on the mechanical conditions at the interface—a finite element analysis with contact. J Biomech 2003;36:1079–86. https://doi.org/10.1016/S0021-9290(03)00114-3.
[6] Li J, Jansen JA, Walboomers XF, van den Beucken JJJP. Mechanical aspects of dental implants and osseointegration: A narrative review. J Mech Behav Biomed Mater 2020;103:103574. https://doi.org/10.1016/j.jmbbm.2019.103574.
[7] Müller BS, Ryang Y-M, Oechsner M, Düsberg M, Meyer B, Combs SE, et al. The dosimetric impact of stabilizing spinal implants in radiotherapy treatment planning with protons and photons: standard titanium alloy vs. radiolucent carbon-fiber-reinforced PEEK systems. J Appl Clin Med Phys 2020;21:6–14. https://doi.org/10.1002/acm2.12905.
[8] Li XA, Chibani O, Greenwald B, Suntharalingam M. Radiotherapy dose perturbation of metallic esophageal stents. Int J Radiat Oncol Biol Phys 2002;54:1276–85. https://doi.org/10.1016/S0360-3016(02)03803-8.
[9] Reft C, Alecu R, Das IJ, Gerbi BJ, Keall P, Lief E, et al. Dosimetric considerations for patients with HIP prostheses undergoing pelvic irradiation. Report of the AAPM Radiation Therapy Committee Task Group 63. Med Phys 2003;30:1162–82. https://doi.org/10.1118/1.1565113.
[10] Ramakrishna S, Mayer J, Wintermantel E, Leong KW. Biomedical applications of polymer-composite materials: a review. Compos Sci Technol 2001;61:1189–224. https://doi.org/10.1016/S0266-3538(00)00241-4.
[11] Wu S, Liu X, Hu T, Chu PK, Ho JPY, Chan YL, et al. A Biomimetic Hierarchical Scaffold: Natural Growth of Nanotitanates on Three-Dimensional Microporous Ti-Based Metals. Nano Lett 2008;8:3803–8. https://doi.org/10.1021/nl802145n.
[12] Mavrogenis A, Dimitriou R, Parvizi J, Babis G. Biology of implant osseointegration. J Musculoskelet Neuronal Interact 2009;9:61–71.
[13] Najeeb S, Zafar MS, Khurshid Z, Siddiqui F. Applications of polyetheretherketone (PEEK) in oral implantology and prosthodontics. J Prosthodont Res 2016;60:12–9. https://doi.org/10.1016/j.jpor.2015.10.001.
[14] Panayotov IV, Orti V, Cuisinier F, Yachouh J. Polyetheretherketone (PEEK) for medical applications. J Mater Sci Mater Med 2016;27:118. https://doi.org/10.1007/s10856-016-5731-4.
[15] Schwitalla A, Müller W-D. PEEK Dental Implants: A Review of the Literature. J Oral Implantol 2013;39:743–9. https://doi.org/10.1563/AAID-JOI-D-11-00002.
[16] Trindade R, Albrektsson T, Galli S, Prgomet Z, Tengvall P, Wennerberg A. Bone Immune Response to Materials, Part I: Titanium, PEEK and Copper in Comparison to Sham at 10 Days in Rabbit Tibia. J Clin Med 2018;7:526. https://doi.org/10.3390/jcm7120526.
[17] Sandler J, Werner P, Shaffer MSP, Demchuk V, Altstädt V, Windle AH. Carbon-nanofibre-reinforced poly(ether ether ketone) composites. Compos Part A Appl Sci Manuf 2002;33:1033–9. https://doi.org/10.1016/S1359-835X(02)00084-2.
[18] Han X, Yang D, Yang C, Spintzyk S, Scheideler L, Li P, et al. Carbon Fiber Reinforced PEEK Composites Based on 3D-Printing Technology for Orthopedic and Dental Applications. J Clin Med 2019;8:240. https://doi.org/10.3390/jcm8020240.
[19] Agostinelli S, Allison J, Amako K, Apostolakis J, Araujo H, Arce P, et al. Geant4—a simulation toolkit. Nucl Instrum Methods Phys Res A 2003;506:250–303. https://doi.org/10.1016/S0168-9002(03)01368-8.
[20] [dataset] Capote R. Phase-space database for external beam radiotherapy. Phase-space database for external beam radiotherapy. International Atomic Energy Agency, Nuclear Data Services 2011. https://www-nds.iaea.org/phsp/photon/Varian_TrueBeam_6MV/.
[21] [dataset] Hubbell JH, Seltzer SM. Tables of X-Ray Mass Attenuation Coefficients and Mass Energy-Absorption Coefficients from 1 keV to 20 MeV for Elements Z = 1 to 92 and 48 Additional Substances of Dosimetric Interest*. 2004.
[22] Bregains JC, Coleman IC, Ares F, Moreno E. Calculating directivities with the two-dimensional Simpson's rule. IEEE Antennas Propag Mag 2004;46:106–12. https://doi.org/10.1109/MAP.2004.1374025.
[23] Larsen RH, Bruland ØS, Hoff P, Alstad J, Lindmo T, Rofstad EK. Inactivation of Human Osteosarcoma Cells In Vitro by 211At-TP-3 Monoclonal Antibody: Comparison with Astatine-211-Labeled Bovine Serum Albumin, Free Astatine-211 and External-Beam X Rays. Radiat Res 1994;139:178–84. https://doi.org/10.2307/3578662.
[24] Hausser H-J, Brenner RE. Phenotypic instability of Saos-2 cells in long-term culture. Biochem Biophys Res Commun 2005;333:216–22. https://doi.org/10.1016/j.bbrc.2005.05.097.
[25] McQuillan DJ, Richardson MD, Bateman JF. Matrix deposition by a calcifying human osteogenic sarcoma cell line (SAOS-2). Bone 1995;16:415–26. https://doi.org/10.1016/8756-3282(95)90186-8.
[26] Schepers RH, Kraeima J, Vissink A, Lahoda LU, Roodenburg JLN, Reintsema H, et al. Accuracy of secondary maxillofacial reconstruction with prefabricated fibula grafts using 3D planning and guided reconstruction. J Craniomaxillofac Surg 2016;44:392–9. https://doi.org/10.1016/j.jcms.2015.12.008.